Projectile-breakup and transfer-reemission reactions in the $^{12}C+^{20}Ne$ system

K. Siwek-Wilczynska,* J. Wilczynski,† C. R. Albiston, Y. Chan, E. Chavez,‡ S. B. Gazes, H. R. Schmidt, and R. G. Stokstad

Nuclear Science Division, Lawrence Berkeley Laboratory, University of California, Berkeley, California 94720

(Received 19 June 1986)

The $^{12}C(^{20}Ne,\alpha\,^{16}O_{g.s.})^{12}C_{g.s.}$, $^{12}C(^{20}Ne,\alpha\,^{20}Ne)^{8}Be_{g.s.}$, and $^{12}C(^{20}Ne,\alpha\,^{12}C)^{16}O^*$ reactions at $E(^{20}Ne)=157$ MeV were studied by using position-sensitive telescopes. It was established that α-^{16}O coincidences in the first reaction result not only from sequential breakup of the projectile, but also from the transfer-reemission process $^{12}C(^{20}Ne,^{16}O_{g.s.})^{16}O^*\rightarrow\alpha+^{12}C_{g.s.}$. Distributions of the excitation energy in the primary reaction products were deduced by calculating respective branching ratios with a Hauser-Feshbach statistical-decay code. It was found that excitation energy is generated in mass transfer reactions quite asymmetrically: it is mostly concentrated in the nucleus that acquires mass, while the "donor" nucleus, on the average, remains cold. These results clearly support the basic concept of "spectator" models of heavy-ion reactions.

I. INTRODUCTION

Heavy-ion reactions with three charged particles in the final state have been of considerable interest in recent years. The application of position-sensitive solid-state detectors has made it possible to measure with precision the relative energies of coincident charged particles and, hence, observe discrete states of sequentially decaying nuclei.[1,2] In the present study, we investigated reactions with three particles in the final state using a "reverse kinematics" reaction, viz., by bombarding a ^{12}C target with ^{20}Ne nuclei. Ternary reactions in the same system have already been studied by Ost *et al.*[3] and Rae *et al.*[4] Given the existing information on ternary reactions in the $^{12}C+^{20}Ne$ system, we concentrated on identifying discrete intermediate states not only in the sequential decay of the projectile, but also in the sequential decay of fragments formed through the transfer of nucleons from the projectile to the target or vice versa. The latter process, which has been referred to as a transfer-reemission reaction,[3] has not been extensively investigated so far, although it is especially interesting because it may selectively lead to high-spin states of specific cluster structures, particularly if the transferred nucleons constitute an alpha particle. In connection with the transfer-reemission reactions, we also investigated ambiguities in the interpretation of ternary reactions, which become especially important at high relative energies. As a part of this study we determine the average excitation energies in the primary reaction products. This information is especially important for understanding mechanisms of generation of excitation energy in heavy-ion reactions.

II. EXPERIMENTAL TECHNIQUE

The experiment was performed with the use of a 157-MeV ^{20}Ne beam produced by the 88-in. cyclotron of the Lawrence Berkeley Laboratory. A 475-$\mu g/cm^2$ C foil was used as a target. Charged particles were detected and identified with telescopes consisting of position-sensitive ΔE and E silicon detectors.[4] The following combinations of silicon detectors were used: 40 μm (ΔE) and 2 mm (E) for two heavy-ion telescopes, and 180 μm (ΔE) and 5 mm (E) for a telescope designated to detect light charged particles (mainly α particles). In each telescope, the ΔE and E detectors provided information on the horizontal and vertical position of the detected particle. Hence, the spatial coordinates of the particle could be determined with an accuracy of about $\pm 0.1°$.

We investigated the following three reactions: $^{12}C(^{20}Ne,\alpha^{12}C)^{16}O$, $^{12}C(^{20}Ne,\alpha^{16}O)^{12}C$, and $^{12}C(^{20}Ne,\alpha^{20}Ne)^{8}Be$. The α-^{12}C, α-^{16}O, and α-^{20}Ne coincidences were analyzed event by event with full reconstruction of momenta and kinetic energies in each three-body event. Hence, the total kinetic energy, $E_{tot}=E_1+E_2+E_3$, and the relative energies in the corresponding subsystem, $E_{rel}(1,2)$ and $E_{rel}(1,3)$, could be calculated. Here the index "1" denotes the α particle, "2" denotes the detected heavy ion (^{12}C, ^{16}O, or ^{20}Ne), and "3" refers to the unobserved third particle (^{16}O, ^{12}C, or ^{8}Be, respectively).

The measurements were taken at two angular configurations of the telescopes: $\langle\theta_1\rangle=26°, \langle\theta_2\rangle=10°$ was the configuration for detecting coincidences at small opening angles ($10.4°<|\theta_1-\theta_2|<21.6°$), and $\langle\theta_1\rangle=26°, \langle\theta_2\rangle=-10°$ was the configuration for measuring coincidences at much wider opening angles ($30.4°<|\theta_1-\theta_2|<41.6°$). The wide-opening-angle geometry of the latter set has not been used so far in experiments involving precise measurements of relative energies. By using this wide-opening-angle configuration, we were able to study sequential-decay processes at high relative kinetic energies with an emphasis on possible ambiguities in the interpretation of these reactions.

III. EXPERIMENTAL RESULTS

A. Introduction

Figure 1 shows spectra of the total kinetic energy, E_{tot}, in the $^{12}C(^{20}Ne,\alpha^{16}O)^{12}C$ reaction for both the wide and

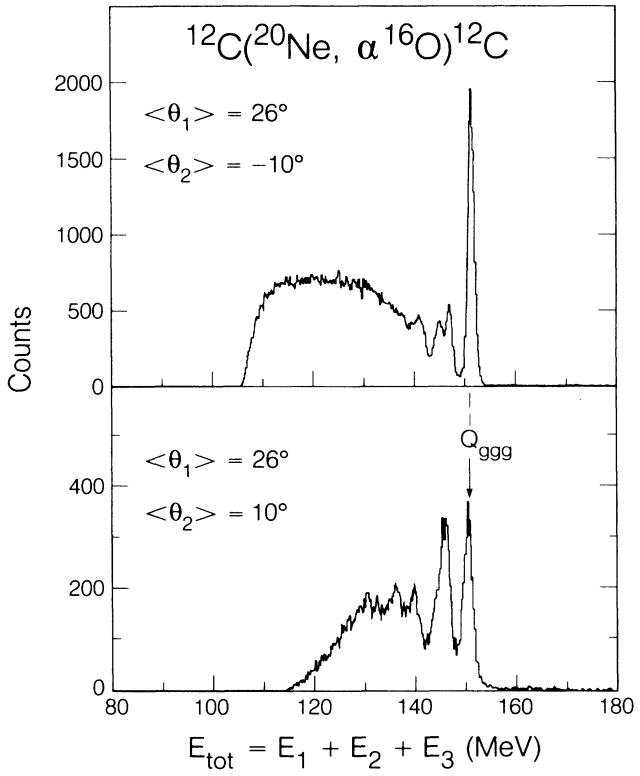

FIG. 1. Spectra of the total kinetic energy, E_{tot}, in the $^{12}C(^{20}Ne,\alpha^{16}O)^{12}C$ reaction for two angular configurations: $\langle\theta_1\rangle = 26°$, $\langle\theta_2\rangle = -10°$ and $\langle\theta_1\rangle = 26°$, $\langle\theta_2\rangle = 10°$. The arrow indicates the energy corresponding to formation of all three final particles in ground states ($Q_{ggg} = -4.73$ MeV). The kinetic energies, E_{tot}, were not corrected for energy losses in the target.

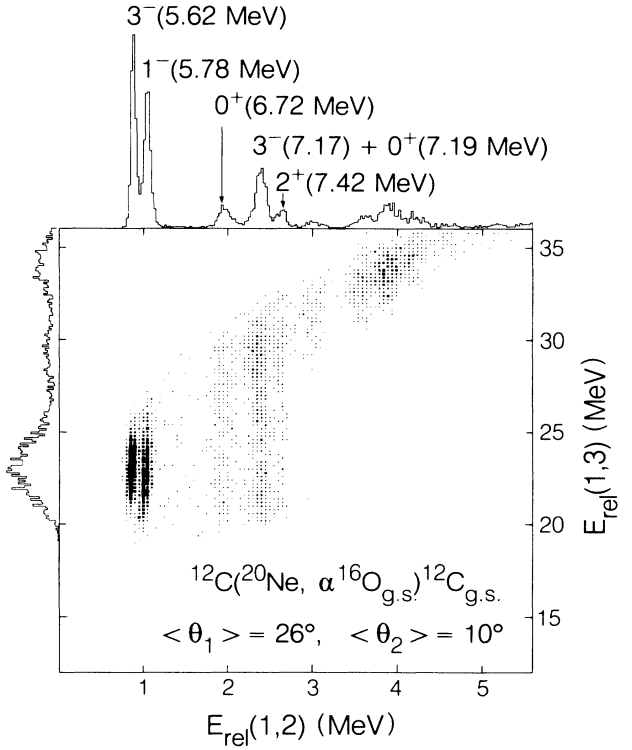

FIG. 2. Scatter plot for the analysis of two-body intermediate states in the reaction with three particles in the final state. Intermediate states only in $E_{rel}(1,2)$ are seen. They correspond to sequential breakup of the projectile.

narrow angular configurations. Both spectra have a sharp peak at $E_{tot} \approx 151$ MeV which corresponds to all three final particles in their ground states ($Q_{ggg} = -4.73$ MeV). The following analysis of the $^{12}C(^{20}Ne,\alpha^{16}O)^{12}C$ reaction is limited to events in the ground state peak. Only with this limitation can the three-body reaction be analyzed unambiguously.

In the following, we present coincidence events in two-dimensional plots as a function of both relative energies $E_{rel}(1,2)$ and $E_{rel}(1,3)$. Concentration of events along a locus of constant $E_{rel}(1,2)$ or constant $E_{rel}(1,3)$ immediately indicates the presence of a two-body intermediate state in the respective subsystem. Such an analysis helps prevent misinterpretations of the coincidence data, especially for large opening angles in which both types of intermediate states may contribute with comparable detection efficiencies.

B. Inelastic scattering and decay

Figure 2 shows the two-dimensional distribution of the α-^{16}O coincidence events from the reaction $^{12}C(^{20}Ne,\alpha^{16}O_{g.s.})^{12}C_{g.s.}$, observed with the small-opening-angle configuration: $\langle\theta_1\rangle = 26°$, $\langle\theta_2\rangle = 10°$. At these detection angles, one sees two-body intermediate states only in $E_{rel}(1,2)$, i.e., in the $\alpha + {}^{16}O$ subsystem. Evidently, the sequential breakup $^{12}C(^{20}Ne,^{20}Ne^* \rightarrow \alpha + {}^{16}O_{g.s.})^{12}C_{g.s.}$ dominates in the class of collisions that can be studied at these detection angles. The observed two-body intermediate states can be easily identified as the known excited states of ^{20}Ne (see top of Fig. 2). As seen from the projected energy spectrum, the 3^- (5.62 MeV) and 1^- (5.78 MeV) states are well resolved. This rather good energy resolution at low relative energies (better than 150 keV) gradually deteriorates with increasing relative energy.

C. Alpha particle stripping and reemission

A similar analysis of the $^{12}C(^{20}Ne,\alpha^{16}O_{g.s.})^{12}C_{g.s.}$ reaction, but for the wide-opening-angle configuration ($\langle\theta_1\rangle = 26°$, $\langle\theta_2\rangle = -10°$), is shown in Fig. 3. At such large opening angles, the products of sequential decay of low-lying excited states in $^{20}Ne^*$ cannot be detected in coincidence. On the other hand, the system can efficiently detect sequential decay from regions of high excitation energy. There is one strong line at $E_{rel}(1,2) = 8.2$ MeV that corresponds to an intermediate state in the $\alpha + {}^{16}O$ subsystem having an excitation energy in ^{20}Ne of $E^* = 12.9$ MeV. It is very interesting that, in addition to the intermediate states in ^{20}Ne, one can clearly see an intermediate state in the $\alpha + {}^{12}C$ subsystem at $E_{rel}(1,3) = 13.6$ MeV, corresponding to an excitation energy of 20.8 MeV in ^{16}O. This intermediate state is

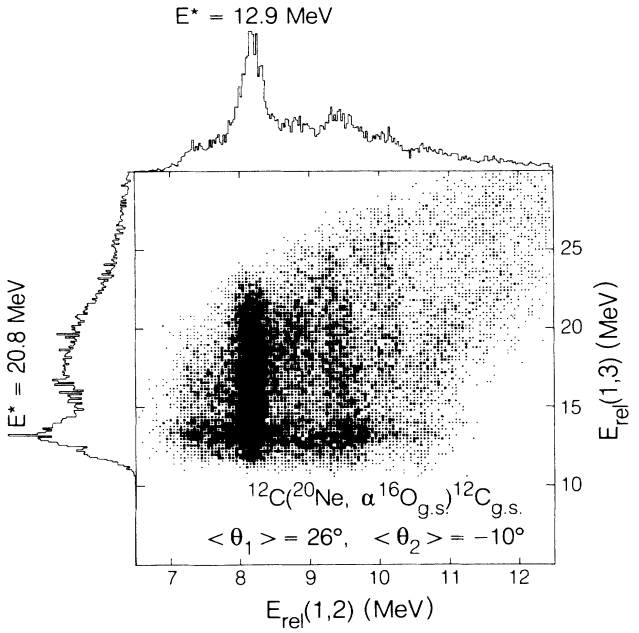

FIG. 3. Same as Fig. 2, except $\langle\theta_1\rangle = 26°$, $\langle\theta_2\rangle = -10°$. Intermediate states in both $E_{rel}(1,2)$ and $E_{rel}(1,3)$ are seen. They correspond to projectile-breakup and transfer-reemission reactions, respectively.

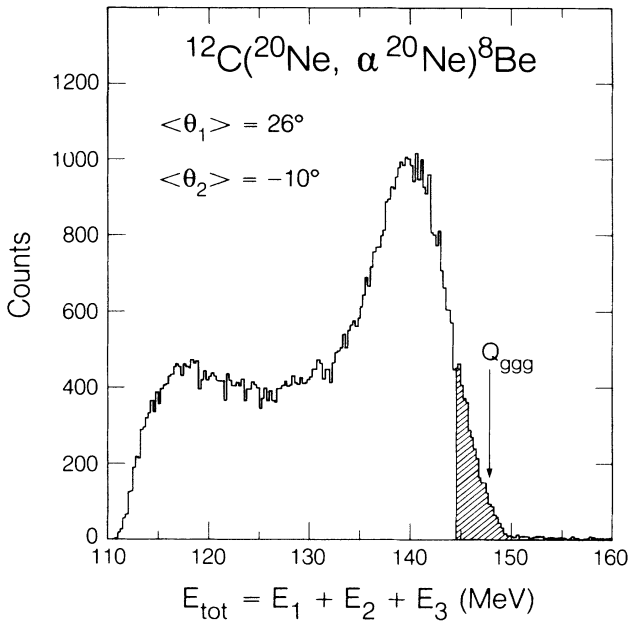

FIG. 4. Spectrum of the total kinetic energy, E_{tot}, in the $^{12}C(^{20}Ne,\alpha^{20}Ne)^{8}Be$ reaction. The arrow indicates the energy corresponding to the $^{12}C(^{20}Ne,\alpha^{20}Ne_{g.s.})^{8}Be_{g.s.}$ reaction ($Q_{ggg} = -7.37$ MeV). Events within the hatched area (above 144 MeV) are believed to comprise both the ground-state reaction and the reaction leading to ^{20}Ne in its first excited state (2^+, 1.63 MeV).

populated in the transfer-reemission reaction $^{12}C(^{20}Ne,^{16}O_{g.s.})^{16}O^* \rightarrow {}^{12}C_{g.s.} + \alpha$, and can be identified with the known 7^- (20.9 MeV) state, which has also been populated very selectively in transfer-reemission reactions induced by ^6Li projectiles.[5]

D. Alpha particle pickup and reemission

We also observed another example of the transfer-reemission process, namely the pickup of an α particle by the projectile to form ^{24}Mg in the reaction $^{12}C(^{20}Ne,^{24}Mg^* \rightarrow \alpha + {}^{20}Ne)^{8}Be$. As is seen from the total-energy spectrum displayed in Fig. 4, there is no well-defined ground-state peak in this reaction. This is because both final nuclei, ^8Be and ^{20}Ne, have relatively low-lying first excited states (2.94 and 1.63 MeV, respectively). The hatched area in Fig. 4 indicates the region around E_{tot} corresponding to the ground-state reaction $^{12}C(^{20}Ne,\alpha^{20}Ne_{g.s.})^{8}Be_{g.s.}$ at $Q_{ggg} = -7.37$ MeV. We estimate that, apart from the ground-state reaction, only the reaction leading to ^{20}Ne in its first excited state (2^+, 1.63 MeV) is contained in this region. The two-dimensional plot in Fig. 5, similar to those of Figs. 2 and 3, shows some structure in $E_{rel}(1,2)$ indicating the presence of intermediate states in the $\alpha + {}^{20}Ne$ subsystem, and does not reveal any distinct intermediate states in the alternative subsystem (1,3). Intermediate states of the latter type would be present if α particles originating from the breakup of the target nucleus, $^{12}C(^{20}Ne,^{20}Ne_{g.s.})^{12}C^* \rightarrow \alpha + {}^{8}Be_{g.s.}$, could be detected. In the following, we assume that all the α-^{20}Ne coincidence events correspond to the (^{20}Ne,$^{24}Mg^*$) reaction.

The spectrum of α-^{20}Ne relative energies, gated by the

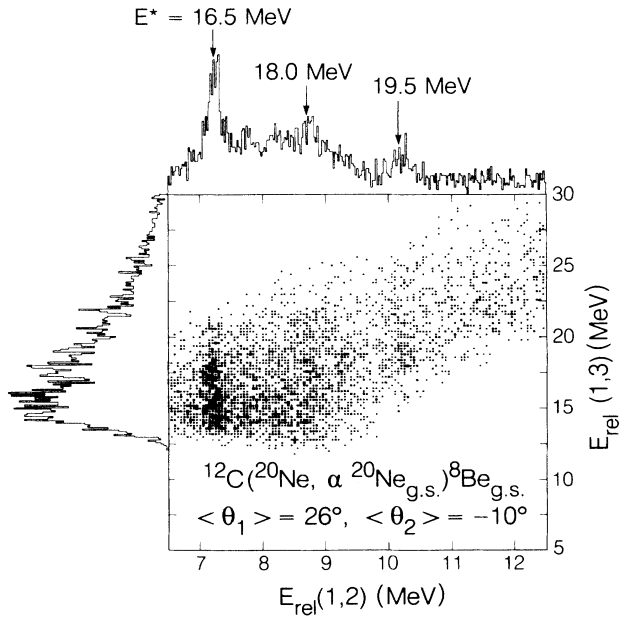

FIG. 5. Scatter plot of the α-^{20}Ne coincidence events from the $^{12}C(^{20}Ne,\alpha^2Ne)^{8}Be_{g.s.}$ reaction at $\langle\theta_1\rangle = 26°$, $\langle\theta_2\rangle = -10°$ gated by the hatched area in Fig. 4. Several intermediate states in $E_{rel}(1,2)$ are seen. They correspond to the transfer-reemission reaction $^{12}C(^{20}Ne,^{24}Mg^* \rightarrow \alpha + {}^{20}Ne)^{8}Be_{g.s.}$. There does not appear to be any evidence for states in the (1,3) system.

ground-state region, is shown in Fig. 6(a). The relative kinetic energies have been converted to excitation energy in ^{24}Mg, $E^*(^{24}\text{Mg}) = E_{\text{rel}}(1,2) + 9.31$ MeV. Peaks in this spectrum can be identified with intermediate states in the transfer-reemission reaction $^{12}\text{C}(^{20}\text{Ne},^{24}\text{Mg}^* \rightarrow \alpha + ^{20}\text{Ne}_{\text{g.s.}})^8\text{Be}_{\text{g.s.}}$. There is one strong peak in the spectrum of Fig. 6 at $E^*(^{24}\text{Mg}) = 16.5 \pm 0.1$ MeV. Besides this, there are two weak peaks of statistical significance at $E^* = 18.0$ and 19.5 MeV. The peak at 16.5 MeV coincides with the 6^+, 16.59 MeV state known from a study of the $^{12}\text{C}(^{16}\text{O},\alpha\alpha)^{20}\text{Ne}_{\text{g.s.}}$ reaction.[6] A similar study of the $^{16}\text{O}(^{12}\text{C},\alpha\alpha\gamma)^{20}\text{Ne}_{\text{g.s.}}$ reaction,[7] however, led to a different conclusion viz., a strong peak at $E^*(^{24}\text{Mg}) = 16.55$ MeV was assigned as a mixture of 8^+ and 9^- states decaying predominantly to the 2^+, 1.63 MeV state in ^{20}Ne. Independent of this particular controversy (which we are not able to resolve), it is clear that we observe the same phenomenon as in the $^{12}\text{C}(^{20}\text{Ne},^{16}\text{O})^{16}\text{O}^*$ reaction discussed previously: a selective population of a high-spin

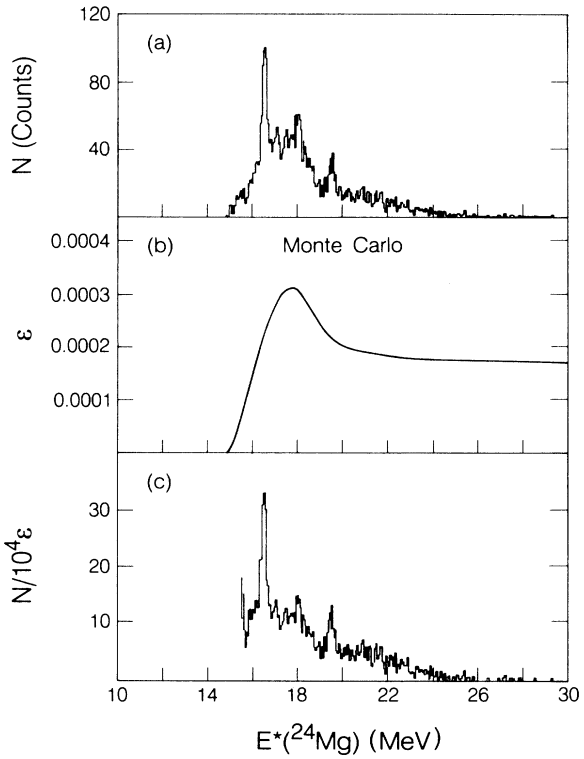

FIG. 6. (a) Spectrum of relative energies in the α-^{20}Ne subsystem from the $^{12}\text{C}(^{20}\text{Ne},\alpha^{20}\text{Ne})^8\text{Be}$ reaction at $\langle\theta_1\rangle = 26°$, $\langle\theta_2\rangle = -10°$ gated by the hatched area in Fig. 4. The spectrum is displayed as a function of excitation energy in ^{24}Mg, $E^*(^{24}\text{Mg}) = E_{\text{rel}}(1,2) + 9.31$ MeV, and interpreted as resulting from the $^{12}\text{C}(^{20}\text{Ne},^{24}\text{Mg}^* \rightarrow \alpha + ^{20}\text{Ne})^8\text{Be}_{\text{g.s.}}$ reaction. Note that due to possible inclusion of the decay to the 2^+ (1.63 MeV) state in ^{20}Ne, the relation between $E^*(^{24}\text{Mg})$ and $E_{\text{rel}}(1,2)$ is not single valued, and, consequently, the displayed spectrum may be slightly distorted. (b) Detection efficiency, ϵ, calculated by Monte Carlo simulation of the $^{12}\text{C}(^{20}\text{Ne},^{24}\text{Mg}^* \rightarrow \alpha + ^{20}\text{Ne}_{\text{g.s.}})^8\text{Be}_{\text{g.s.}}$ reaction. (c) Spectrum of (a) corrected for the detection efficiency. For the assignments of the observed peaks, see text.

state in the transfer-reemission reaction. This essential feature of transfer-reemission reactions was first observed by Artemov *et al.*[5,8] in (^{6}Li,αd) reactions, and investigated using ^{12}C beams by Rae *et al.*[9]

IV. EXCITATION ENERGY OF PRIMARY PRODUCTS

A. Efficiency correction

It is interesting to compare the shapes of the excitation energy spectra of the primary products in both of the nuclear processes discussed so far: inelastic scattering (^{20}Ne,^{20}Ne*), and pickup of an α particle (^{20}Ne,^{24}Mg*). In order to do so, the spectra in question have to be corrected for the efficiency of detecting the coincidence events. The detection efficiency was calculated by using the Monte Carlo method. The following two assumptions were made in these calculations: (i) primary fragments decay isotropically in their c.m. frame, and (ii) angular distributions of the primary (unbound) fragments are the same as those measured inclusively for the respective bound particles in the equivalent range of Q values. Experimental detection thresholds have been accounted for in these calculations.

Figure 6(b) shows the curve of detection efficiency, ϵ, calculated for the $^{12}\text{C}(^{20}\text{Ne},^{24}\text{Mg}^* \rightarrow \alpha + ^{20}\text{Ne}_{\text{g.s.}})^8\text{Be}_{\text{g.s.}}$ reaction. The spectrum of Fig. 6(a) corrected for this detection efficiency is shown in Fig. 6(c). Results of the same procedure applied to the data on the projectile-breakup reaction $^{12}\text{C}(^{20}\text{Ne},^{20}\text{Ne}^* \rightarrow \alpha + ^{16}\text{O}_{\text{g.s.}})^{12}\text{C}_{\text{g.s.}}$ at $\langle\theta_1\rangle = 26°$, $\langle\theta_2\rangle = -10°$ are shown in Fig. 7. [As seen from Fig. 3, the projected spectrum includes events corresponding to a reaction other than $^{12}\text{C}(^{20}\text{Ne},^{20}\text{Ne}^*)^{12}\text{C}_{\text{g.s.}}$. However, these provide only a small, structureless contribution that does not affect the shape of the spectrum in Fig. 7(c).] Apart from the strong peak at $E^* = 12.9$ MeV, another peak at $E^* = 12.0$ MeV stands out in the efficiency-corrected spectrum of Fig. 7(c). [The latter peak is almost invisible in the experimental spectrum in Fig. 7(a) due to the rapidly falling efficiency in this near-to-threshold region.] Since there are several levels in ^{20}Ne at this range of excitation energies, we cannot identify the observed resonances with absolute certainty. Most likely, they can be identified with the known[10] states at $E^* = 11.96$ MeV ($J^\pi = 1^-$) and 12.83 MeV ($J^\pi = 1^-$). The spin assignment of the latter state was recently reported by Caskey.[11]

B. The distribution of excitation energy

Comparison of the spectra from Figs. 6(c) and 7(c) provides important information on the mechanism of generating excitation energy in fast (nonequilibrium) heavy-ion reactions. Since the configuration of detectors is the same for both reactions, the respective primary reaction products (^{20}Ne* and ^{24}Mg*) are emitted at comparable angles of about 3°, i.e., close to the classical grazing angle, $\theta_{\text{gr}} = 4.5°$. In both reactions, the α-decay branch to the ground state is defined for each value of excitation energy by the gate on the ground-state peak. Therefore, the primary distribution of excitation energy in the parent fragment can be deduced by calculating (within a statistical model) the branching ratio of this specific channel of α decay. The Hauser-Feshbach calculations have been done

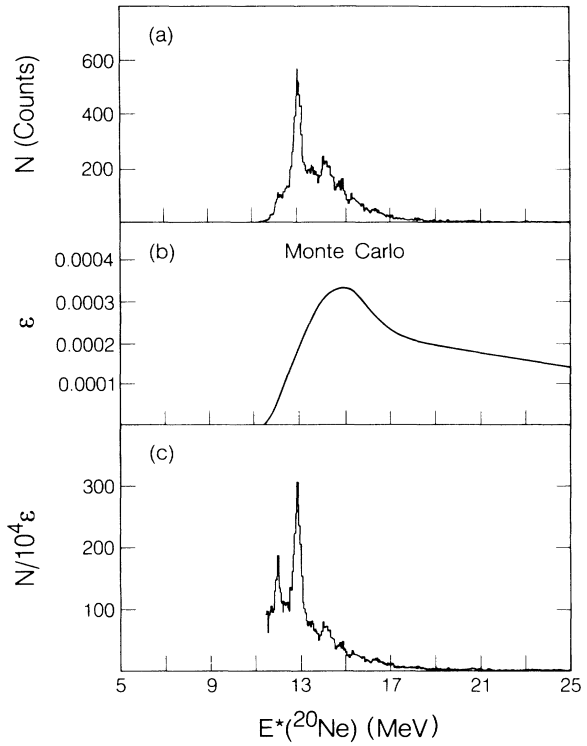

FIG. 7. (a) Spectrum of relative energies in the α-^{16}O subsystem from the $^{12}C(^{20}Ne,\alpha^{16}O_{g.s.})^{12}C_{g.s.}$ reaction at $\langle\theta_1\rangle = 26°$, $\langle\theta_2\rangle = -10°$, displayed as a function of excitation energy in ^{20}Ne, $E^*(^{20}Ne) = E_{rel}(1,2) + 4.73$ MeV. (b) Detection efficiency, ϵ, calculated by Monte Carlo simulation of the $^{12}C(^{20}Ne,^{20}Ne^* \rightarrow \alpha + {}^{16}O_{g.s.})^{12}C_{g.s.}$ reaction. (c) Spectrum of Fig. 6(a) corrected for the detection efficiency. For the assignments of the observed peaks, see text.

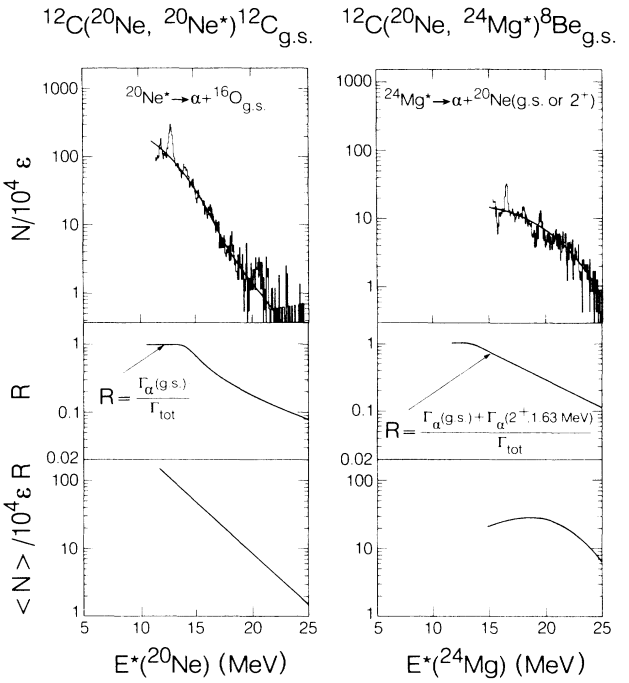

FIG. 8. Comparison of the $^{12}C(^{20}Ne,^{20}Ne^*)^{12}C_{g.s.}$ and $^{12}C(^{20}Ne,^{24}Mg^*)^{8}Be_{g.s.}$ reactions. Spectra of excitation energy from Figs. 7(c) and 6(c) (corrected for detection efficiency) are plotted in logarithmic scale on the top. Branching ratios, R, of the experimentally selected α-decay channels, calculated with the Hauser-Feshbach statistical-decay code STATIS (Ref. 12) are shown in the middle panel. The deduced distributions of excitation energy of the primary products, $^{20}Ne^*$ and $^{24}Mg^*$, are shown in the lower panel. They correspond to the smooth dependence of N on E^* as plotted together with the histograms on the top.

by using the statistical-decay code STATIS.[12] Individual excited states in the daughter nuclei reached by n, p, and α decay were used in the calculations. The calculated branching ratios, R, of α decay to the experimentally selected final states relative to all possible n, p, or α decays are shown in the middle part of Fig. 8.

The experimental spectra of Figs. 6(c) and 7(c) are presented (on a logarithmic scale) in Fig. 8 above the results of the Hauser-Feshbach calculations. The smooth curves drawn through the data will be used to obtain the average distributions of excitation energy. Since the experimental distributions are proportional to the numerator of the ratio R, one can obtain spectra of primary excitations for both reactions in question by dividing the smoothed spectrum on the top of Fig. 8 by the respective values of R. The results of this division are shown in the lower part of Fig. 8.

The deduced distributions of primary excitations in the $^{12}C(^{20}Ne,^{20}Ne^*)^{12}C_{g.s.}$ and $^{12}C(^{20}Ne,^{24}Mg^*)^{8}Be_{g.s.}$ reactions are strikingly different. In the inelastic-scattering channel (lower left-hand corner of Fig. 8), the distribution falls exponentially with increasing excitation energy. If this dependence were extrapolated to lower excitation energies, the average excitation energy in the inelastic scattering would be $\langle E^*\rangle = 2.8$ MeV.

On the other hand, in the four-nucleon pickup reaction $^{12}C(^{20}Ne,^{24}Mg^*)^{8}Be_{g.s.}$ the distribution of the primary excitation has a maximum at $E^* \approx 18$ MeV and, consequently, the average excitation is very likely close to that value. This result clearly shows that generation of excitation energy is associated with the transfer of mass, a basic assumption of any "spectator" model, and, specifically, the optimum-Q-value model of Siemens *et al.*[13] As a matter of fact, the spectator models imply a specific partition of the excitation energy generated by the transfer of mass. Namely, these models implicitly assume that transferred nucleons leave the parent nucleus unexcited and bring their individual momenta into the receiving fragment. Consequently, the nucleus that accepts the transferred mass gets all the excitation energy released in the reaction. Certainly this is only an idealized picture, suggesting a certain trend in average excitation energies of the two reaction partners.

Some qualitative indications in support of this picture have already been reported in Ref. 14. Results of recent work of Schmidt *et al.*[15] on reactions in a more asymmetric system are also consistent with this concept.

Our results on the four-nucleon pickup reaction $^{12}C(^{20}Ne,^{24}Mg^*)Be_{g.s.}$ show that the nucleus that accepted the transferred mass (^{24}Mg) indeed is highly excited, on

the average, but it should be pointed out that this particular reaction does not provide information about the most probable excitation of the donor nucleus (^{8}Be), since only events corresponding to the ground state of ^{8}Be have been selected by our gate on E_{tot}. Therefore, it is interesting to supplement results on the $^{12}C(^{20}Ne,^{24}Mg^*)^8Be_{g.s.}$ reaction with information on another reaction in which the same massive fragment (an α cluster) is transferred the other way, viz., the $^{12}C(^{20}Ne,^{16}O)^{16}O$ reaction.

Figure 9 shows the spectrum of the total kinetic energy for the events involving α-^{12}C coincidences. (As previously, three-body kinematics has been applied to produce this spectrum.) The peak at $E_{tot} \approx 151$ MeV corresponds to a reaction with all three reaction products in their ground states ($Q = -4.73$ MeV), i.e., the $^{12}C(^{20}Ne,\alpha^{12}C_{g.s.})^{16}O_{g.s.}$ reaction. There are three other peaks in this spectrum, corresponding to excitation energies in the final system of about 6, 11, and 15 MeV. They correlate quite well with the excited states in ^{16}O which are known to be selectively populated in α-transfer reactions, such as $^{12}C(^7Li,t)^{16}O^*$ (see Ref. 16). Therefore, at least in the range of not-too-high excitation energies (i.e., below 20 MeV), the observed events can be interpreted as resulting from the α-transfer reaction $^{12}C(^{20}Ne,^{16}O^*)^{16}O^*$. Thus we conclude that peaks in the spectrum in Fig. 9 correspond to the excited states in the acceptor nucleus (target residue), while the excited donor nucleus (projectile residue) undergoes α decay to the ground state of ^{12}C. It should be pointed out that in the discussed region of low excitation energies none of the detected α particles can originate from the decay of the acceptor nucleus because, as seen from Fig. 3, the lowest excited state in the target-residue ^{16}O nucleus that is detectable above our experimental threshold is the 7^- state at 20.9 MeV.

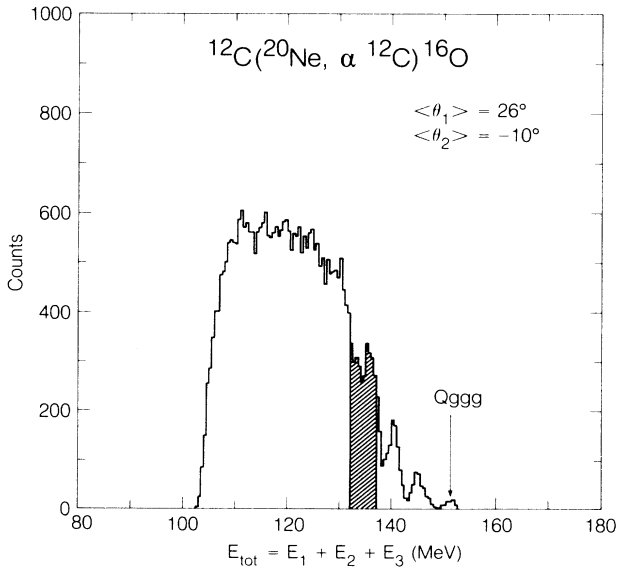

FIG. 9. Spectrum of the total kinetic energy, E_{tot}, in the $^{12}C(^{20}Ne,\alpha^{12}C)^{16}O$ reaction. The arrow indicates the energy corresponding to the $^{12}C(^{20}Ne,\alpha^{12}C_{g.s.})^{16}O_{g.s.}$ reaction ($Q_{ggg} = -4.73$ MeV). The region indicated by the hatched area was chosen for analysis of the primary distribution of excitation energies.

We analyzed the distribution of relative kinetic energies in the α-^{12}C system for a limited range of E_{tot} (shown in Fig. 9 as the hatched area). The choice of this range of excitation energies (from 14 to 19 MeV) was dictated by two factors: (i) We wanted to closely approach the optimum kinematical conditions for the α-transfer reaction $^{12}C(^{20}Ne,^{16}O)^{16}O$. The optimum Q value[13,17] for this reaction is about -19 MeV. This corresponds to a combined excitation energy of both final ^{16}O nuclei of about 21 MeV. (ii) By limiting the excitation energy of the acceptor nucleus to 19 MeV, we eliminated the possibility of detecting α particles from the decay of the acceptor nucleus. Moreover, our gate includes the peak at 15-MeV excitation that very likely corresponds to the group of 5^- and 6^+ states in the acceptor ^{16}O nucleus, which have been observed in the $^{12}C(^7Li,t)^{16}O^*$ reaction.[16] Therefore, we conclude that the events in the hatched region in Fig. 9 predominantly originate from the $^{12}C(^{20}Ne^{16}O^* \rightarrow \alpha + ^{12}C)^{16}O^*$ reaction.

Figure 10(a) shows the α-^{12}C relative-energy spectrum gated by the hatched region in the distribution of E_{tot} in Fig. 9. As discussed above, this spectrum results from α decay of the projectile residues produced in the $(^{20}Ne,^{16}O^*)$ reaction. The detection efficiency ϵ [Fig. 10(b)] was calculated by simulating the $^{12}C(^{20}Ne,^{16}O^* \rightarrow \alpha + ^{12}C)^{16}O^*$ reaction with the Monte Carlo method (within the same gate in E_{tot}).

We reconstructed the primary distribution of excitation energy the same way as for the two other reactions discussed previously. The relative-energy spectrum was divided by the corresponding numbers of the efficiency, ϵ, and the branching ratio,

$$R = [\Gamma_\alpha(\text{g.s.}) + \Gamma_\alpha(2^+, 4.44 \text{ MeV})]/\Gamma_{tot} .$$

(The 2^+ state at 4.44 MeV is the only bound excited state in ^{12}C.) In this reconstruction [Fig. 10(c)], we assumed the same relation between the measured relative kinetic energy and the excitation energy as for the ground-state decay: $E^* = E_{rel} + 7.16$ MeV. Therefore, events corresponding to the decay to the 2^+ state ($E^* = E_{rel} + 11.60$ MeV) are located in our spectrum at too-low energies, thus causing an effective shift of the reconstructed spectrum, especially at higher excitation energies at which the decay to excited states becomes more competitive. This effect, however, does not influence the slope of the reconstructed spectrum at the lowest measured relative energies.

The spectrum of primary excitations in the donor ^{16}O nucleus, displayed in Fig. 10(c), falls off very rapidly with increasing excitation energy. Any reasonable extrapolation of this distribution towards lower excitation energies leads to an estimate of the average excitation of the ^{16}O-donor nucleus well below 12 MeV. For example, if the distribution is extrapolated with the same exponential slope as that observed for the lowest measured relative energies (6—10 MeV), the average excitation energy would be about 1.5—2.0 MeV. At the same time, the average excitation of the ^{16}O-acceptor nucleus (for events within the hatched area in Fig. 9) is about 16 MeV. (We averaged excitation energies of the acceptor nucleus for the two decay modes of the donor nucleus in the proportion given by

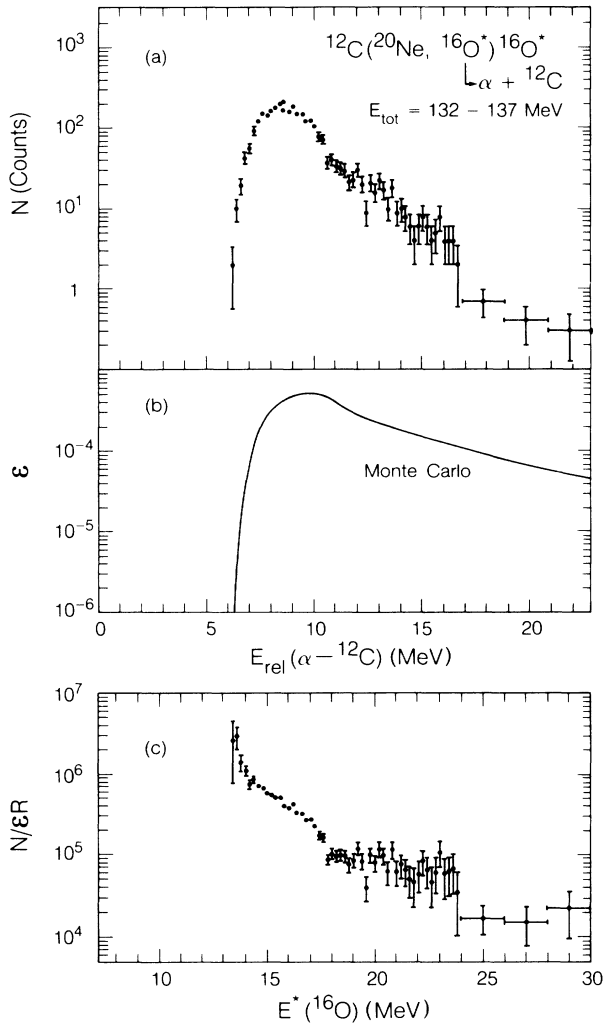

FIG. 10. (a) Spectrum of relative kinetic energies in the α-^{12}C subsystem from the $^{12}C(^{20}Ne,\alpha^{12}C)^{16}O^*$ reaction at $\langle\theta_1\rangle = 26°$, $\langle\theta_2\rangle = -10°$, gated by the range of E_{tot} as shown in Fig. 9. (b) Detection efficiency, ϵ, calculated by Monte Carlo simulation of the $^{12}C(^{20}Ne,^{16}O^* \rightarrow \alpha + ^{12}C)^{16}O^+$ reaction. (c) The deduced distribution of excitation energy of the projectile residue (donor nucleus) in the $^{12}C(^{20}Ne,^{16}O^*)^{16}O^*$ reaction. The branching ratio, $R = [\Gamma_\alpha(\text{g.s.}) + \Gamma_\alpha(2^+, 4.44\ \text{MeV})]/\Gamma_{tot}$, for α decay to the only two bound states of ^{12}C was calculated with the Hauser-Feshbach statistical-decay code STATIS (Ref. 12).

the Hauser-Feshbach calculation.)

In addition to the analysis presented in Fig. 10, we investigated shapes of the relative energy spectra for α-^{12}C coincidences gated by other regions of E_{tot}, specifically those corresponding to lower excitation energies of the acceptor nucleus. Independent of the excitation of the acceptor nucleus, the excitation-energy spectrum of the donor nucleus has always a similar shape: it rapidly decreases with increasing E_{rel}, as in Fig. 10(a). This indicates a very low average value of the donor's excitation energy, even in those cases where a higher excitation of the donor nucleus would be required to match the optimum Q value.

Our analysis shows that in the $^{12}C(^{20}Ne,^{16}O^*)^{16}O^*$ reaction the excitation energy of the residual donor nucleus, on the average, is considerably lower than the excitation energy of the acceptor nucleus. Since both primary products have the same mass, the observed asymmetry in the partition of the excitation energy must arise as a consequence of the direction of mass transfer, and, certainly, cannot be influenced by different level densities of the reaction products, as might be the case in reactions of very asymmetric systems.

High average excitations of the nuclei that acquire the transferred mass may explain, at least partly, the very low cross sections for pickup reactions to bound states, which are usually measured in inclusive experiments. For example, in the four-nucleon pickup reaction $^{12}C(^{20}Ne,^{24}Mg^*)^8Be_{g.s.}$ we observed a most probable excitation of the ^{24}Mg nucleus of about 18 MeV, i.e., well above the particle-instability threshold for this nucleus ($S_\alpha = 9.31$ MeV).

V. SUMMARY

In summary, using position-sensitive detectors we investigated reactions in the ^{20}Ne + ^{12}C system with three charged particles in the final state. By plotting coincidence events in two dimensions, $E_{rel}(1,2)$ vs $E_{rel}(1,3)$, we were able to identify two-body intermediate states in respective subsystems involving particles 1 and 2 or 1 and 3. We have found that at certain angular configurations both types of intermediate states may be present. Therefore, experiments with poor resolution in the determination of the relative energies should be interpreted with caution. For example, we established that α-^{16}O coincidences in the $^{12}C(^{20}Ne,\alpha^{16}O_{g.s.})^{12}C_{g.s.}$ reaction result from two sequential processes: the breakup of ^{20}Ne* following inelastic scattering (which is a "standard" interpretation of the coincidence experiments), and the transfer-reemission reaction $^{12}C(^{20}Ne,^{16}O_{g.s.})^{16}O^* \rightarrow \alpha + ^{12}C_{g.s.}$ We also studied another transfer-reemission process, namely the $^{12}C(^{20}Ne,^{24}Mg^* \rightarrow \alpha + ^{20}Ne)^8Be_{g.s.}$ reaction. In both these transfer-reemission reactions, high-spin states are preferentially excited. By using a Monte Carlo simulation for determining detection efficiency and by performing Hauser-Feshbach statistical calculations, we were able to reconstruct primary distributions of excitation energy in the $^{12}C(^{20}Ne,^{20}Ne^*)^{12}C_{g.s.}$, $^{12}C(^{20}Ne,^{24}Mg^*)^8Be_{g.s.}$, and $^{12}C(^{20}Ne,^{16}O^*)^{16}O^*$ reactions. These results clearly show that the generation of excitation energy is associated with transfer of mass. In addition, the results of the latter two reactions give evidence for a very asymmetric generation of the excitation energy in the mass transfer reactions: The excitation energy is mostly concentrated in the acceptor nucleus, while the donor nucleus, on the average, remains cold. This result strongly supports the basic concept of "spectator" models of heavy-ion reactions.

This work was supported by the U.S. Department of Energy under Contract DE-AC03-76SF00098.

*Permanent address: Institute of Experimental Physics, Warsaw University, 00-681 Warsaw, Poland.
†Permanent address: Institute for Nuclear Studies, 05-400 Swierk/Warsaw, Poland.
‡Permanent address: Instituto de Fisica, Universidad Nacional Autónoma de México, Apartado Postal 20364, México 01000, Distrito Federal, México.

[1]J. van Driel, S. Gonggrijp, R. V. F. Janssens, R. H. Siemssen, K. Siwek-Wilczynska, and J. Wilczynski, Phys. Lett. **98B**, 351 (1981).
[2]W. D. M. Rae, A. J. Cole, A. Dacal, R. Legrain, B. G. Harvey, J. Mahoney, M. J. Murphy, R. G. Stokstad, and I. Tserruya, Phys. Lett. **105B**, 417 (1981).
[3]R. Ost, S. Kox, A. J. Cole, N. Longequeue, J. J. Lucas, J. Menet, and J. B. Viano, Nucl. Phys. **A361**, 453 (1981).
[4]W. D. M. Rae, A. J. Cole, B. G. Harvey, and R. G. Stokstad, Phys. Rev. C **30**, 158 (1984).
[5]K. P. Artemov, V. Z. Goldberg, I. P. Petrov, V. P. Rudakov, I. N. Serikov, and V. A. Timofeev, Phys. Lett. **37B**, 61 (1971).
[6]A. Gobbi, P. R. Maurenzig, L. Chua, R. Hadsell, P. D. Parker, M. W. Sachs, D. Shapira, R. Stokstad, R. Wieland, and D. A. Bromley, Phys. Rev. Lett. **26**, 396 (1971).
[7]R. W. Zurmuhle, D. P. Balamuth, L. K. Fifield, and J. W. Noe, Phys. Rev. Lett. **29**, 795 (1972).
[8]K. P. Artemov, V. Z. Goldberg, I. P. Petrov, V. P. Rudakov, I. N. Serikov, V. A. Timofeev, and P. R. Christensen, Nucl. Phys. **A320**, 479 (1979).
[9]W. D. M. Rae, S. C. Allcock, S. Marsh, and B. R. Fulton, Phys. Lett. **156B**, 167 (1985).
[10]F. Ajzenberg-Selove, Nucl. Phys. **A300**, 1 (1978).
[11]G. Caskey, Phys. Rev. C **31**, 717 (1985).
[12]R. G. Stokstad, Wright Nuclear Structure Laboratory Report No. 52, Yale University, 1972 (unpublished).
[13]P. J. Siemens, J. P. Bondorf, D. H. E. Gross, and F. Dickmann, Phys. Lett. **36B**, 24 (1971).
[14]K. Siwek-Wilczynska, R. A. Blue, L. H. Harwood, R. M. Ronningen, H. Utsunomiya, and J. Wilczynski, Phys. Rev. C **32**, 1450 (1985).
[15]H. R. Schmidt, S. B. Gazes, Y. Chan, R. Kamermans, and R. G. Stokstad, Phys. Lett. **180B**, 9 (1986).
[16]M. E. Cobern, D. J. Pisano, and P. D. Parker, Phys. Rev. C **14**, 491 (1976).
[17]J. Wilczynski, in Proceedings of the International Conference on Nuclear Physics, Florence, 1983 (invited papers), Vol. II, p. 305 (unpublished).